Journal of Materials Chemistry B

Accepted Manuscript

ROYAL SOCIETY OF CHEMISTRY

www.rsc.org/materialsB

Cite this: DOI: 10.1039/c0xx00000x

www.rsc.org/xxxxxx

ARTICLE TYPE

Insulin-Loaded Hydroxyapatite Combined with Macrophage Activity to Deliver Insulin for Diabetes Mellitus

Yen-Jye Shyong[a], Rui-Feng Lin[d], Hung-Sheng Soung[e], Hung-Hsuan Wei[a], Yu-Sheng Hsueh[a], Kuo-Chi Chang[b,*], Feng-Huei Lin[a,c,*]

Received (in XXX, XXX) Xth XXXXXXXXX 20XX, Accepted Xth XXXXXXXXX 20XX
DOI: 10.1039/b000000x

We aimed to develop a diabetes mellitus (DM) treatment that could be administered by intramuscular (IM) injection and lasted more than 3 days. The objective was to load insulin into the lattice space of hydroxyapatite (HAP) to prevent its release based on a concentration gradient or detachment from surface. while the insulin releasing in the study had to combine with the cellular activity. To avoid insulin denaturation during insulin-loaded HAP (insHAP) synthesis, we developed a single-step insHAP synthesis method by hydrolysis of brushite. X-ray diffraction (XRD), Fourier transform infrared (FTIR) spectroscopy, scanning electron microscopy (SEM), and transmission electron microscopy (TEM) results suggested that insulin could be loaded into the HAP crystal lattice. After IM administration in rats with DM, synthesized insHAP is thought to be engulfed by macrophages, escape from lysosome/endosome hybrids following disruption by osmotic pressure, and pumped into the extracellular space before entering the blood circulation by diffusion. In rats with DM, normal blood glucose level was maintained for 4 days after a single IM injection of synthesized insHAP particles. Thus, insHAP may provide a breakthrough in insulin delivery for DM treatment, and may also be used to deliver fluorescent proteins, antibodies, and anticancer drugs.

1 Introduction

Diabetes mellitus (DM) is a metabolic disease in which an individual experiences high blood glucose levels.[1] DM can be divided into 2 types. In type 1 DM, the insulin-producing pancreatic beta islet cells are destroyed by the individual's autoimmune system, which leads to an inheritable shortage or even complete absence of insulin production. Type 2 DM patients are insulin resistant or have relatively low insulin production. In this group of individuals, malfunction of pancreatic beta cells occurs and may be due to disease, age, or damage. Regardless of type, DM patients usually need exogenous insulin to maintain blood glucose within the normal range. However, insulin is a protein-based drug that cannot pass through the gastrointestinal (GI) tract undamaged. Therefore, transdermal and/or subcutaneous injection are now the gold standards for insulin delivery.[2] However, DM patients must alternate the injection site day-to-day because low recovery rates in wound healing are associated with DM. Therefore, daily insulin delivery by subcutaneous routes is not a convenient method.

Researchers have tested several methods over the past 2 decades in order to overcome the inconvenience associated with current delivery methods. The goal of current research is to achieve long-term delivery methods. Allo- and xeno-islet transplantations with a semi-permeable membrane for immune-isolation have been developed for long-term delivery of insulin.[3] However, the immune-isolation function of membranes is lost within 3 months of surgery because the pores become blocked with fibrous encapsulation.[4–6] Auto-stem cells have been harvested and purified for the same purpose; however, this method remains far off clinical application. In addition, the cell isolation, purification, and regulation techniques are very tedious, time consuming, expensive, and associated with easy loss of phenotype before the whole process is completed.[7,8] Computer-programmed bio-artificial pancreases are available on the market and are used to determine blood glucose levels and use real-time data to deliver the appropriate dose of insulin through the peritoneal cavity. The approach requires the patient to extracorporeally bear a device with an insulin cartridge, controller, sensor, and subcutaneous delivery catheter at all times; this approach is not associated with good quality of life.[9–11]

Polymers have been developed to enclose insulin and allow it to bypass the GI tract degradation during oral administration; however, these were not effective in the clinical setting and have not been commercialized. Although several pharmaceutical companies have developed and marketed different kinds of long-acting formulation delivered by subcutaneous injection, these still require once-daily administration.[12–15] In the present study, we designed a long-acting formula capable of releasing insulin over 4 days following intramuscular (IM) injection, in which cellular activity would regulate constant release.

Hydroxyapatite (HAP), which is the major inorganic mineral of bone and teeth, has superior biocompatibility and osteo-integration and has been used successfully as bone graft. HAP has been used for drug delivery purposes, and drugs are generally loaded onto the surface. However, this method has always been associated with a high ratio of initial drug release rather than constant release since drug release is based on diffusion or concentration gradient.[16–18] In the research, HAP has served as an insulin carrier; however, instead of loading insulin on the surface

of the HAP, it could be loaded into the lattice spaces of HAP during its synthesis.[19–22] After insulin-loaded HAP (insHAP) is prepared, it could be injected by the IM route. Insulin would only be released from interstitial sites when defense cells in the body take up insHAP particles to acidic lysosomes. The prepared particles would be completely dissolved within a few hours in a lysosome/endosome hybrid that may form in high concentrations of Ca^{2+} and PO_4^{3-} and be broken down due to osmotic pressure. Insulin would then escape from the degraded lysosome/endosome hybrid into the cytoplasm, be pumped out into the extracellular space, and finally diffuse into the circulating blood (Scheme 1). The developed particles would be slowly engulfed by defense cells at the injection site to achieve constant insulin release and regulate blood glucose levels.

2 Results

2.1. Materials Characterization

Figure 1A and 1B show the X-ray diffraction (XRD) pattern of pure HAP and insHAP. All the characteristic peaks were matched to the standard pattern of HAP according to the diffraction standards detailed on JCPD card 09-0432. We observed that the crystal structure of synthesized insHAP was HAP with a hexagonal structure and no second phase or impurity could be traced from the pattern. The characteristic peak of (002) at 2θ = 25.67° on the XRD pattern of insHAP was shifted to the left about 0.26° from the standard pattern of HAP at 2θ = 25.93°. The major peak of (211) at 2θ = 31.61° on the XRD pattern of insHAP was shifted to the left about 0.21° from the peak at 2θ = 31.82° of the standard pattern. Peak (300) at 2θ = 32.58° on the XRD pattern of insHAP was shifted to the left about 0.32° from the peak at 2θ = 32.90° of the standard pattern. We believed that inter-planer space of (002), (211), and (300) in insHAP was larger than that found in standard HAP due to insulin loading. The length of the a-axis and c-axis of insHAP was calculated as 9.46 and 6.94, respectively. In addition, most of the diffraction peaks on the pattern of insHAP were broadened and rough, which might contribute towards the lower crystallinity when compared with pure HAP. These results are summarized in Table 1.

The morphology of insHAP examined under scanning electron microscope (SEM) is shown in Figure 2A. The needle-like grains aggregated into particles to form a spherulite structure. The chemical composition of the synthesized insHAP was semiquantified by SEM-accessorized energy dispersive spectrophotometer (EDS), where carbon and nitrogen could be traced in the synthesized particles with the weight ratio of 6.6% and 4.27%, respectively, as shown in Figure 2B and Table 2. The results of EDS and XRD can be regarded as part of the evidence to prove that insulin molecules were successfully loaded into the inter-planer space of insHAP crystals.

Figure 3A and 3B show transmission electron microscopy (TEM) images of pure HAP and insHAP, respectively. Grains of pure HAP and synthesized insHAP were all needle-like in shape; however, synthesized insHAP grains had a longer c-axis, like an extension. Figure 3C shows the lattice image of pure HAP with a d-spacing of 0.33 nm that could be identified as plane (002). Figure 3D is the lattice image of synthesized insHAP and shows the absence of a clear lattice on the TEM picture due to lower crystallinity resulted from insulin addition. The electronic diffraction pattern of pure HAP is shown in Figure 3E. The polycrystalline ring pattern can be clearly examined and identified as the specific crystal plane to match the standard HAP. Figure 3F is the electronic diffraction pattern of insHAP that was identical to the pure HAP. However, the ring pattern of insHAP was broader and blurry because of lower crystallinity. Some of rings were too broadened and overlapping to be identified clearly. Therefore, only 3 rings, (002), (202), and (222) were assigned.

Figure 4(a), 4(b) and 4(c) show the Fourier transform infrared (FTIR) spectroscopy patterns of standard HAP, pure insulin and insHAP, respectively. Where figure 4(a) shown absorption bands at 3570 cm^{-1}, 1040–1100 cm^{-1}, and 565–605 cm^{-1}; these were assigned as the –OH stretching vibrations mode, PO_4^{3-} stretching vibrations mode, and PO_4^{3-} bending vibrations mode, respectively. These were the absorption bands for HAP. In the FTIR pattern for pure insulin, absorption bands were detected at wavelengths 3485 cm^{-1}, 1200 cm^{-1}, 1000 cm^{-1}, 780 cm^{-1}, and 400–470 cm^{-1}. These bands were the result of functional groups found in insulin: –NH stretching vibrations mode, -C-OH stretching vibrations mode, C-N stretching vibrations mode, Aryl of -NH2 bending vibrations mode, and S-S, respectively. Figure 4 (c) was the FTIR pattern of insHAP; where all the absorption bands could be assigned to insulin or HAP. Insulin functional groups were labeled as I, II, III, IV, and V, respectively.

Size distribution of insHAP analyzed from the zeta-sizer is shown in Figure 5A. Particle size was in the range of 550–865 nm, with a polydispersity index of 0.369. The zeta potential of pure HAP and insHAP was 7.68 mV and -3.32 mV, respectively, as shown in Figure 5B and 5C.

2.2. Insulin Loading

As shown in the thermogravimetric analysis (TGA) curve in Figure 6(a), only minor weight loss was observed around 100°C due to water evaporation for pure HAP. Figure 6(b) shows the TGA curve for pure insulin. The initial weight loss at 100°C was due to water evaporation. The next loss at 225°C was associated with the temperature of insulin decomposition. The TGA curve for insHAP is shown in Figure 6(c). A weight loss of 7.4% observed at 225°C was indicated by the curve, and was proportional to the percentage of insulin loaded in HAP. The results demonstrated that insulin could be loaded into the interstitial space of the HAP lattice at an approximate weight ratio of 7.4%.

2.3. Insulin Release Profile

The ultraviolet-visible (UV-vis) absorption curve of Humulin® R between wavelengths of 260 and 300 nm demonstrated that λ_{max} was located at 276 nm with an absorption rate of 0.396 (Figure 7A). Figure 7B shows the insulin release profile curve of insHAP at a wavelength of 276 nm under phosphate buffer saline. In a normal physiological environment with pH 7.4, 12% of insulin was released from insHAP in the first few hours; no insulin was released from insHAP thereafter. At pH 4.0, which represents the lysosome/endosome hybrid environment, 92% of insulin was released from insHAP within 2 hours, with 100% released by day 3.

2.4. Cell Viability, Cytotoxicity, and Cellular Uptake

The results of the WST-1 assay of 3T3 cells with insHAP on day 1 and day 3 are shown in Figure 8A. No significant differences were detected between the experimental groups with insHAP concentration in 0.05, 0.1, 0.2, and 0.4 mg/mL and the control group. Similar findings were observed with the lactate dehydrogenase (LDH) assay as shown in Figure 8B. Therefore, no cytotoxicity was associated with insHAP.

RAW-264.7 (control) TEM samples double-stained with uranyl acetate (UA) and lead citrate (LC) are shown in Figure 9A. Lysosome/endosome hybrids are indicated with red arrows. Figure 9B shows the TEM sample of RAW-264.7 cells cultured with insHAP for 24 h. Evidence of insHAP particles uptake by RAW-264.7 cells and enclosure in the lysosome/endosome hybrid was observed under TEM. Note that white circles indicated with red arrows are lysosome/endosome hybrids, while the black-colored needle-like particles are insHAP.

2.5. *In Vivo* Study

Daily blood glucose measurements were taken, and as shown in Figure 10, blood glucose levels of all DM rats were greater than 250 mg/dL during the experimental period. This is in contrast with blood glucose levels that fell within the range of 50–125 mg/dL in all normal rats (NC group). Glucose levels of DM rats treated with basal insulin (DM + basal insulin group) decreased to 109.75 ± 4.72 mg/dL on day 1; however, glucose levels returned to 278.75 ± 5.74 mg/dL on day 2, and were elevated above 250 mg/dL thereafter. In DM rats treated with IM insHAP (DM + insHAP), blood glucose levels on day 1 were 230.00 ± 7.07 mg/dL. On day 2, blood glucose levels decreased to 109.50 ± 7.14 mg/dL, and were further suppressed to 74.25 ± 18.77 mg/dL and 67.25 ± 21.00 mg/dL on day 3 and day 4, respectively. Although blood glucose levels rebounded to 98.75 ± 2.99 mg/dL and 129.5 ± 25.32 mg/dL on day 5 and day 6, respectively, these values were considered within the normal range. However, after day 7, blood glucose levels increased to within the range observed in DM rats.

3 Discussion

The crystal size of synthesized pure HAP and insHAP could be evaluated from the respective XRD patterns (Figure 1A and 1B) by Scherr's formula:[23]

$$t = (0.9\lambda \times 180°) \div (\beta \cos\theta\beta)$$

where t is the particle size, λ is the wavelength of x-ray, β is the full-width at half maximum, and θ_β is Bragg's angle at the measured peak. If plane (002) was used, the average crystal size of synthesized insHAP was approximately 89 nm, and this finding was in agreement with the result of TEM examination (Figure 3A and 3B). The grain of pure HAP was in needle-like shape with c-axis along the long axis of the grain identified as plane (002) that was shown in Figure 3C. The grain of synthesized insHAP, looks a shorter grain due to a much slower rate of grain growth resulting from the insulin addition. In summary from the TEM and XRD examination: (1) HAP with insulin addition (insHAP) cause to grain looks shorter than that of HAP without insulin addition (pure HAP). (2) HAP with insulin addition would interfere the crystal growth resulting in poor crystallinity; this could be proved by XRD pattern and TEM electronic diffraction pattern. (3) Poor crystal growth and lower crystallinity of insHAP lead to smaller grain size resulting in a much less needle-like morphology; that made grains much easier to be stacked into agglomeration.

Particles analyzed by the zeta-sizer were in the range of 550–865 nm; aggregation was due to high surface energy as shown in Figure 2A.[24] The particle size of the developed insHAP was in the optimum range for cell uptake.[25] The synthesized particles were designed to be delivered to the human body by an IM route. The particles would be gradually engulfed by marcrophages (Figure 9B) and quickly dissolved in the acidic lysosome/endosome hybrid. The concentration of Ca^{2+} and PO_4^{3-} in the hybrid would increase and create sufficient osmotic pressure to break down the lysosome/endosome hybrid; potentially allowing loaded insulin escape from the lysosome/endosome hybrid by enzyme degradation. The high concentration of Ca^{2+} ions would also cause exocytosis, releasing insulin into the extracellular space, and finally diffusing into the blood circulation system to decrease blood glucose to normal levels.[26] The lysosome/endosome hybrids in the RAW-264.7 control group (Figure 9A) were clean inside and much smaller compared with RAW-264.7 cells (Figure 9B). This evidence is suggestive that following uptake of insHAP, rising osmotic pressure inside the lysosome/endosome hybrid will cause the hybrid to inflate and finally break down.

The length of a-axis and c-axis of insHAP calculated by Bragg's law were 9.46 and 6.94 (Table 1), respectively. Based on the insHAP XRD pattern (Figure 1B), the inter-planer space of (002), (211), and (300) are considered larger than that observed in standard HAP. The volume of the crystal lattice of insHAP would therefore be larger than that of pure HAP. The volume increase might be due to insulin loading to the interstitial space of the lattice causing it to expand. The findings of EDS and XRD provide evidence that insulin molecules were successfully loaded into the inter-planer space of insHAP crystals (Figure 2B and Table 2).

The insHAP zeta-potential of -3.32 mV was more negative than the 7.68-mV value obtained with pure HAP (Figure 5B and 5C). It is well known that insulin is a protein-based molecule produced in the beta cells of the pancreatic islets. It is firstly synthesized as the single-chain 86–amino acid precursor, preproinsulin. Subsequent proteolytic processing splices the amino-terminal peptide giving rise to proinsulin. The mature insulin molecule is a hexamer with 51 residues and a net charge of -12 at neutral pH. The insulin molecule contains many negative charge residues, for instance, aspartic acid and glutamic acid. These residues would be attracted by the HAP surface, resulting in HAP with more negative charge because of charge compensation.[27]

The surface adsorption would give rise to the initial burst observed in the *in vitro* release profile (Figure 7B). In the neutral solution, 12% of insulin released from insHAP occurred during the first few hours, and could be explained by the initial burst due to surface adsorption. No insulin was released from insHAP thereafter because insulin molecules were loaded in the lattice of HAP. When insHAP was exposed to pH 4.0, as seen in the lysosome/endosome hybrid, 92% of insulin was released within 2 hours and 100% released by day 3. This could be due to insHAP

quickly dissolving in the acidic condition to release insulin.

The aggregation of insHAP was necessary for 2 reasons. The first reason was that it provided a more effective size for macrophage uptake. The second reason was to create inter-granular space to increase the surface area for insulin adsorption, and subsequently increase insulin loaded in the HAP. This is illustrated by its micro-structure with adequate pore size and porosity as shown in Figure 2A.

In the animal study (Figure 10), blood glucose in DM rats administered IM insHAP were as elevated as DM rats on day 1. Blood glucose levels fell to within the normal range on day 2, and this was maintained for 4 days. insHAP delivered by IM requires uptake by macrophages, escape from lysosome/endosome hybrid complexes that are disrupted due to osmotic pressure, pumping out into the extracellular space, and diffusion into the blood circulation. The lack of an obvious fall in blood glucose following insHAP treatment on day 1 could be explained by the time required to accomplish this process. Considering that blood glucose levels rose on day 7 to levels observed in DM rats, we can assume that all the injected insHAP is digested by macrophages 6 days after IM administration.

4 Conclusions

This study has demonstrated a long-lasting insulin release system lasting more than 4 days when administered by IM injection. Insulin loaded into HAP lattice space is not dependent on drug delivery based on a concentration gradient or detachment from surface adsorption. In order to avoid insulin denaturation during insHAP synthesis, we developed a single-step insHAP synthesis by hydrolysis of brushite. We believe that insulin can be loaded into the HAP crystal lattice, and insHAP particle size was in the optimum range for cell uptake. Synthesized insHAP delivered by IM to DM rats is engulfed by macrophages, escapes from lysosome/endosome hybrids disrupted by osmotic pressure, is pumped into the extracellular space, and diffuses into the circulating blood circulation. Synthesized insHAPs have the potential to provide a more convenient approach to regulating blood glucose levels in patients with DM.

5 Experimental section

5.1. **Reagents and Cells**

Calcium chloride ($CaCl_2$, Sigma-Aldrich, St. Louis, USA) and disodium phosphate dihydrate ($Na_2HPO_4 \cdot 2H_2O$, Sigma-Aldrich, St. Louis, USA) were used as sources of Ca^{2+} and PO_4^{3-} ions, respectively. Regular human insulin, Humulin® R, was obtained from Eli Lilly (Indianapolis, USA), at a concentration of 100 IU/mL. Sodium hydroxide (NaOH, MERCK, Darmstadt, Germany) and hydrochloric acid (HCl, Sigma-Aldrich, St. Louis, USA) were used to adjust the pH value during material preparation. 3T3 cells and RAW-264.7 were purchased from Bio-resource Collection and Research Center (FIRDI, Hsin-Chu City, Taiwan). 3T3 cells served as target cells for the evaluation of cytotoxicity and viability. RAW-264.7, a type of mouse macrophage cells, was used as a model cell to examine under TEM how defense cells internalize the developed particles *in vitro*.

5.2. **Synthesis of insHAP**

Insulin-loaded brushite (insDCPD) was firstly co-precipitated as an intermediate compound described as follows. Briefly, 10 mL of 5 M $CaCl_2$ aqueous solution was mixed with 20 mL Humulin® R by magnetic stirrer; and then slowly added to 10 mL of 7 M Na_2HPO_4 aqueous solution to precipitate insDCPD at room temperature.[28–30] Prepared insDCPD was then recrystallized into non-stoichiometric insHAP after treatment with excessive Na_2HPO_4; NaOH was added drop-wise to adjust the pH value to pH 8 while magnetic stirring at 100 rpm. The precipitate was collected by centrifugation and washed with deionized water 3 times. The synthesized particles were freeze-dried and stored at 4°C for later experiments.

5.3. **Materials Characterization and Analysis**

Storage particles were mounted on the sample holder of an XRD instrument (Rigaku Geigerflex, Tokyo, Japan) for crystal structure identification. The XRD pattern was obtained at 30 kV and 20 mA with 2θ range of 10°–60° at a count time of 0.5 s/step. The 2θ shift, lattice constant, d-spacing and crystallinity were calculated based on the pattern by XRD equipped software, MDI Jade 5.0.[31]

The morphology of the synthesized particles was observed under SEM (Philips XL30, Amsterdam, Netherlands) with accelerating voltage of 15 kV. Particles were mounted on the sample stage of the SEM and coated with platinum-film by sputtering physical vapor deposition. The purpose of the platinum film was to increase the imaging resolution and prevent u-desired charge accumulation.[32] The chemical composition was analyzed by SEM-equipped EDS.

TEM (FEI Tecnai G2 20, Hillsboro, USA) was used to further identify the crystal structure and the grain size of the synthesized particles. The insHAP particles suspended in double-distilled H_2O was dropped onto the Formvar-coated copper grid (Ted Pella Inc., Redding, CA) and then air dried at room temperature. The morphology, electronic diffraction pattern, and lattice imaging of the prepared particles were obtained by TEM with an accelerating voltage of 200 kV.[33]

The absorbed spectrum of insHAP was characterized by FTIR spectroscopy (JASCO 410, Tokyo, Japan) to analyze functional groups. The particles were mixed with KBr in a ratio of 1:9 and pressed into a disk with a pressure of 10 MPa. All the spectra were collected in the range of 400–4000 cm^{-1} wavenumber at a scanning rate of 400 nm/min.[34]

The particle size and zeta-potential of insHAP were detected under water by a Zeta-sizer (Malvern, Worcestershire, UK) operated at 10–70°C (±0.1°C). The detected range of particle size was between 2 nm and 8 μm.[35]

5.4. **Efficiency of Insulin Loading**

TGA of insHAP was performed by TGA–differential thermal analysis (TA Instrument SDT2960, New Castle, Germany) in the atmosphere of nitrogen gas from 30°C to 600°C with a heating rate of 5°C/min.[36] The degree of weight loss during thermal analysis correlated with the amount of insulin loaded in insHAP.

5.5. Insulin Release Profile

The release profile of insulin from insHAP was determined using a UV-vis spectrometer (JASCO V-670, Tokyo, Japan) at pH 7.4 and pH 4.0 intended to mimic conditions in the physiological environment and in the lysosome/endosome hybrid, respectively.[37] Then, 100 mg insHAP was immersed in 5 mL of phosphate-buffered saline (PBS, pH 7.4) and incubated at 37°C for 24 h. The supernatant was collected by centrifugation and insulin concentration measured by UV-vis by the absorbance at the wavelength 276.12. Insulin concentration was determined by interpolation from the calibration curve. Then, the insHAP precipitate was refilled with 5 mL of PBS and incubated at 37°C. The process was repeated every 24 h until 7 days.

5.6. Evaluation of Cell Viability and Cytotoxicity

Cell viability of insHAP was evaluated by WST-1 assay (BioVision, Milpitas, USA) under ISO-10993 guidelines. Briefly, 1 mg of synthesized particles were immersed in 10 mL Dulbecco's modified Eagle's medium (Sigma-Aldrich, St. Louis, USA) supplemented with 10% fetal bovine serum (Gemini Bioproducts, Calabasas, CA) and 10% biotin for 24 h. The synthesized particles were centrifuged and discarded, while the extraction solution was reserved for later cell culture experiments. 3T3 cells were seeded onto 96-well petri dishes at a density of 10^4 cells per well. The extraction solution and fresh medium were mixed in the ratio of 1:1 and added to the culture well. WST-1 assays were measured by an enzyme-linked immunosorbent assay reader at the wavelength of 450 nm.[38]

The cytotoxicity of the synthesized particles was evaluated by LDH assay (Promega, Madison, USA). The synthesized particles were treated with the same immersion process used to prepare the extraction solution. The 3T3 cells were seeded onto 96-well petri dishes at the same seeding density used in the WST-1 assay. The results of LDH assays were measured at the wavelength of 490 nm.[39]

5.7. Observation of Phagocytosis of Particles Taken Up by RAW-264.7 Cells

RAW-264.7 macrophages were seeded onto 9-cm petri dishes at a density of 10^5 cells/dish and cultured for 3 days until confluence. The cells were then treated with 500 μM insHAP (0.24 mg/mL) for 24 h. Cells were then washed thoroughly with chilled PBS, pelleted by centrifugation, fixed with 2.5% glutaraldehyde overnight, and post-fixed in 1% osmium tetroxide solution for 1–2 h. Cells were then rinsed 3 times with 0.2 M PBS and rinsed with PBS dehydrated in ethanol (35%, 50%, 70%, 85%, 90%, 95%, and 100%). Cell cryotomy was performed, and images were recorded by TEM (Jeol, JEM-1200EX II, Tokyo, Japan) operated at 100 kV to observe how the particles were internalized by macrophages.[40]

5.8. Animal Experiments

All animal experiments were performed in compliance with the relevant laws and institutional guidelines, and have been approved by the Animal Center of National Taiwan University.

DM was induced in Wistar rats by depriving the rats of food overnight and then administering 65 mg/kg streptozotocin by intraperitoneal injection. After DM induction, the non-fasting blood glucose (NFBG) was measured everyday by using a glucose meter. The successful induction of type 1 DM was confirmed by 2 consecutive measurements of blood glucose greater than 250 mg/dL.[41] The basal insulin of 2.5 IU LANTUS® (insulin glargine, Sanofi, Paris, France) administered by IM injection was considered the control group. Considering that 1 IU is equivalent to 0.0347 mg, then 2.5 IU is the equivalent of 0.08675 mg insulin. According to the TGA results, insulin is loaded into HAP at a ratio of 7.4%. Therefore, control rats received 0.08675/7.4% of insulin, which equates to 1.1723 mg. According to clinical administration of insulin therapy, more insulin should be delivered since it is partly degraded in the physiological environment. In the present study, a total of 8.206 mg (1.1723 mg per day for 7 days) of insHAP in 0.3 mL PBS was delivered to each rat by IM injection. Rats had *ad libitum* access to food during the experimental period, and were offered excess food. The tail vein was punctured with a blood glucose meter to measure NFBG in rats consecutively for 10 days.

5.9. Statistical Analysis

Data are expressed as mean ± standard deviation (S.D.). Statistical analysis was performed by ANOVA, and differences were considered statistically significantly different when $p < 0.05$.

Acknowledgment

We would like to gratitude to Animal Center of National Taiwan University for their profession help in animal study. We also appreciate National Science Council, Taiwan, and National Health Research Institute, Taiwan, for the financial support to the research and make the research possible.

Notes and references

[a] *Institute of Biomedical Engineering, National Taiwan University, No. 1, Sec. 4, Roosevelt Road, Taipei 10617, Taiwan*
[b] *Department of Chemical Engineering and Biotechnology, National Taipei University of Technology, No. 1, Sec. 3, Chung-Hsiao E. Road, Taipei, 10608, Taiwan*
[c] *Division of Medical Engineering, National Health Research Institute, No. 35, Keyan Rd., Zhunan, Miaoli County, 35053, Taiwan*
[d] *Department of Neurosurgery, Mackay Memorial Hospital, No. 92, Sec. 2, Zhongshan N. Rd., Taipei City 10449, Taiwan.*
[e] *Department of Psychiatry, Yuan-Shan br. of Taipei Veteran General Hospital, No. 301, Sec. 1, Subin Rd., Suao Township, Yilan County 27047, Taiwan (R.O.C.)*
*The two corresponding authors contributed equally to this work.

1 G. Puavilai, S. Chanprasertyotin and A. Sriphrapradaeng, *Diabetes Res. Clin. Pract.*, 1999, **44**, 21-26.
2 Z. Qi, C. Yamamoto, N. Imori, A. Kinukawa, K. Yang, G. Yanai, E. Ikenoue, Y. Shen, Y. Shirouzu, A. Hiura, K. Inoue and S. Sumi, *Cell Transplant*, 2012, **21**, 525-534.
3 A. Gangemi, P. Salehi, B. Hatipoglu, J. Martellotto, B. Barbaro, J. B. Kuechle, M. Qi, Y. Wang, P. Pallan, C. Owens, J. Bui, D. West, B. Kaplan, E. Benedetti and J. Oberholzer, *Am. J. Transplant*, 2008, **8**, 1250-1261.
4 T. Wang, I. Lacik, M. Brissova, A. V. Anilkumar, A. Prokop, D. Hunkeler, R. Green, K. Shahrokhi and A. C. Powers, *Nat. Biotechnol.*, 1997, **15**, 358-362.
5 M. K. Lee and Y. H. Bae, *Adv. Drug Deliv. Rev.*, 2000, **42**, 103-120.
6 K. C. Yang, C. C. Wu, S. Sumi, C. L. Tseng, Y. H. S. Wu, T. F. Kuo and F. H. Lin, *Pancreas*, 2010, **39**, 444-451.
7 J. C. Voltarelli, C. E. B. Couri, A. B. P. L. Stracieri, M. C. Oliveira, D.

A. Moraes, F. Pieroni, M. Coutinho, K. C. R. Malmegrim, M. C. Foss-Freitas, B. P. Simoes, M. C. Foss, E. Squiers and R. K. Burt, *JAMA*, 2007, **297**, 1568-1576.
8 M. A. Hussain, Lancet, 2004, **364**, 203-205.
9 E. Renard, *Curr. Opin. Pharmacol*., 2002, **2**, 708-716.
10 K. Kumareswaran, M. L. Evans and R. Hovorka, *Expert Rev. Med. Devices*, 2009, **6**, 401-410.
11 M. Vix, D. Mutter, N. Jeandidier, S. Boivin, M. Pinget and J. Marescaux, *Ann. Chir*., 1994, **48**, 991-997.
12 T. Ikoma, H. Kobayashi, J. Tanaka, D. Walsh and S. Mann, *J. Struct. Biol*., 2003, **142**, 327-333.
13 Y. Liu, E. B. Hunziker, N. X. Randall, K. de Groot and P. Layrolle, *Biomaterials* 2003, **24**, 65-70.
14 J. F. Villanueva-Espinosa, M. Hernandez-Esparza and F. A. Ruiz-Trevino, *Ind. Eng. Chem. Res*., 2001, **40**, 3563-3569.
15 S. Dasgupta, S. S. Banerjee, A. Bandyopadhyay and S. Bose, *Langmuir*, 2010, **26**, 4958-4964.
16 K. Ijntema, W. J. M. Heuvelsland, C. A. M. C. Dirix and A. P. Sam, *Int. J. Pharm*., 1994, **112**, 215-224.
17 M. Itokazu, W. Yang, T. Aoki, A. Ohara and N. Kato, *Biomaterials*, 1998, **19**, 817-819.
18 Y. Mizushima, T. Ikoma, J. Tanaka, K. Hoshi, T. Ishihara, Y. Ogawa and A. Ueno, *J. Control Release*, 2006, **110**, 260-265.
19 S. Ishihara, T. Matsumoto, T. Onoki, M.H. Uddin, T. Sohmura and A. Nakahira, *Acta Biomaterialia*, 2010, **6**, 830-835.
20 T.Y. Liu, S.Y. Chen, D.M. Liu and S.C. Liou, *J Control Release*, 2005, **107**, 112–121.
21 V. Uskokovic and D.P. Uskokovic, *J Biomed Mater Res B*, 2010, **96B**, 152–191.
22 P. Yang, Z. Quan, C. Li, X. Kang, H. Lian and J. Lin, *Biomaterials*, 2008, **29**, 4341–4347.
23 C. Krishnaraj, E. G. Jagan, S. Rajasekar, P. Selvakumar, P. T. Kalaichelvan and N. Mohan, *Colloid Surf. B-Biointerfaces*, 2010, **76**, 50-56.
24 G. Zuo, C. Liu, H. Luo, F. He, H. Liang, J. Wang and Y. Wan, *J. Appl. Polym. Sci*., 2009, **113**, 3089-3094.
25 M. Rabinovitch, *Trends Cell Biol*., 1995, **5**, 85-87.
26 U. Becherer, T. Moser, W. Stühmer and M. Oheim, *Nature Neuroscience*, 2003, **6**, 846-853.
27 K. Yang, Z. Qi, C. Wu, Y. Shirouza, F. Lin, G. Yanai and S. Sumi, *Biochem. Biophys. Res. Commun*., 2010, **393**, 818-823.
28 M. T. Fulmer and P. W. Brown, *J. Mater. Sci. Mater. Med*., 1998, **9**, 197-202.
29 F. Fievet, J. P. Lagier, B. Blin, B. Beaudoin and M. Figlarz, *Solid State Ionics*, 1989, **32-33**, 198-205.
30 S. K. Garg, J. A. Carmain, K. C. Braddy, J. H. Anderson, L. Vignati, M. K. Jennings and H. P. Chase, *Diabetic Med*., 1996, **13**, 47-52.
31 J. W. Gilman, C. L. Jackson, A. B. Morgan and R. Harris, *Chem. Mater*., 2000, **12**, 1866-1873.
32 E. Ruska, *Microsc. Acta. Suppl*., 1980, **5**, 1-140.
33 B. D. Busbee, S. O. Obare and C. J. Murphy, *Adv. Mater*., 2003, **15**, 414-416.
34 R. M. Silverstein and J. O. Rodin, *Microchem. J*., 1965, **9**, 301-308.
35 F. Booth, *Nature*, 1948, **161**, 83-86.
36 C. D. Doyle, *J. Appl. Polym. Sci*., 1961, **5**, 285-292.
37 H. Mansur, R. Oréfice, M. Pereira, Z. Lobato, W. Vasconcelos and L. Machado, *Spectroscopy*, 2002, **16**, 351-360.
38 T. Mosmann, *J. Immunol. Methods*, 1983, **65**, 55-63.
39 D. B. Mitchell, K. S. Santone and D. Acosta, *J. Tissue Cult. Meth*., 1980, **6**, 113-116.
40 R. Shukla, V. Bansal, M. Chaudhary, A. Basu, R. R. Bhonde and M. Sastry, *Langmuir*, 2005, **21**, 10644-10654.
41 T. Krupin, S. R. Waltman, D. W. Scharp, C. Oestrich, S. D. Feldman, B. Becker, W. F. Ballinger and P. E. Lacy, *Invest. Ophthalmol. Vis. Sci*., 1979, **18**, 1185-1190.

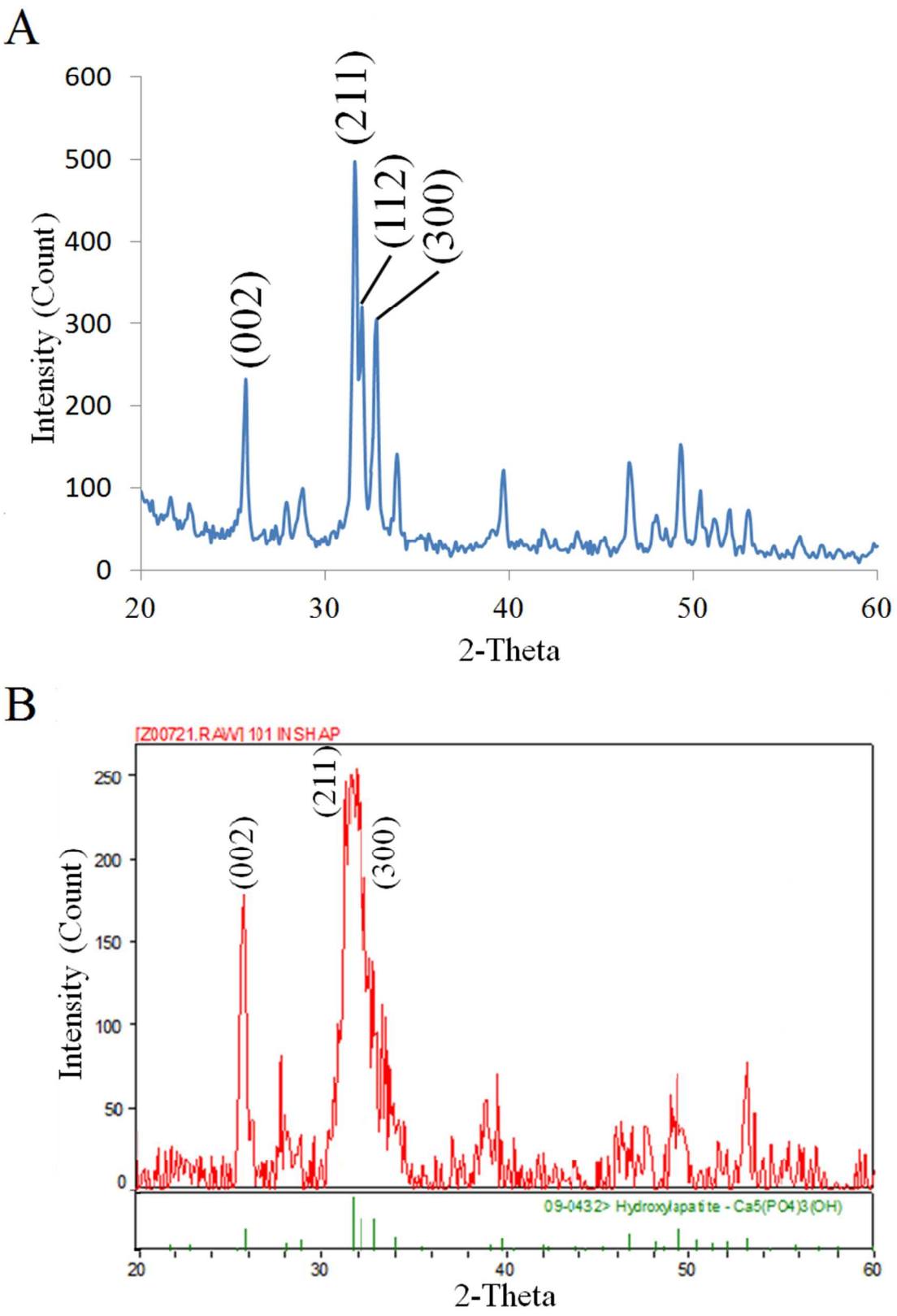

Figure 1. Figure caption. X-ray diffraction pattern of (A) pure HAP and (B) insHAP. Due to insulin loading, the characteristic peaks of insHAP were shifted to the left compared with pure HAP. However, all characteristic peaks still matched the standard HAP pattern as determined by JCPD card (09-0432).

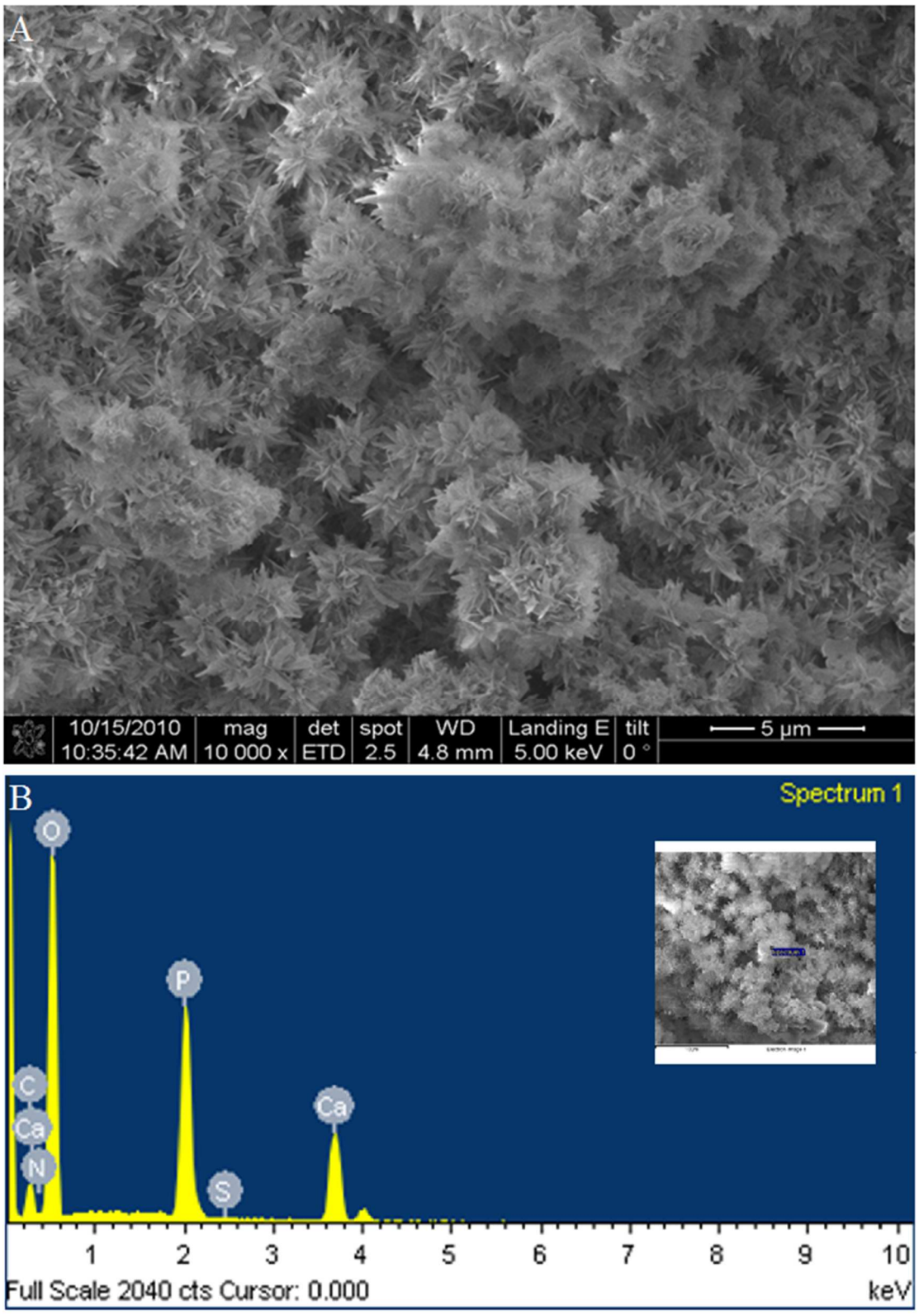

Figure 2. Figure caption. (A) Morphology of insHAP examined under SEM. The needle-like grains aggregated into particles to form a spherulite structure. (B) Chemical composition of synthesized insHAP was semiquantified by EDS. Sulfur, carbon, and nitrogen were traced in the synthesized particles.

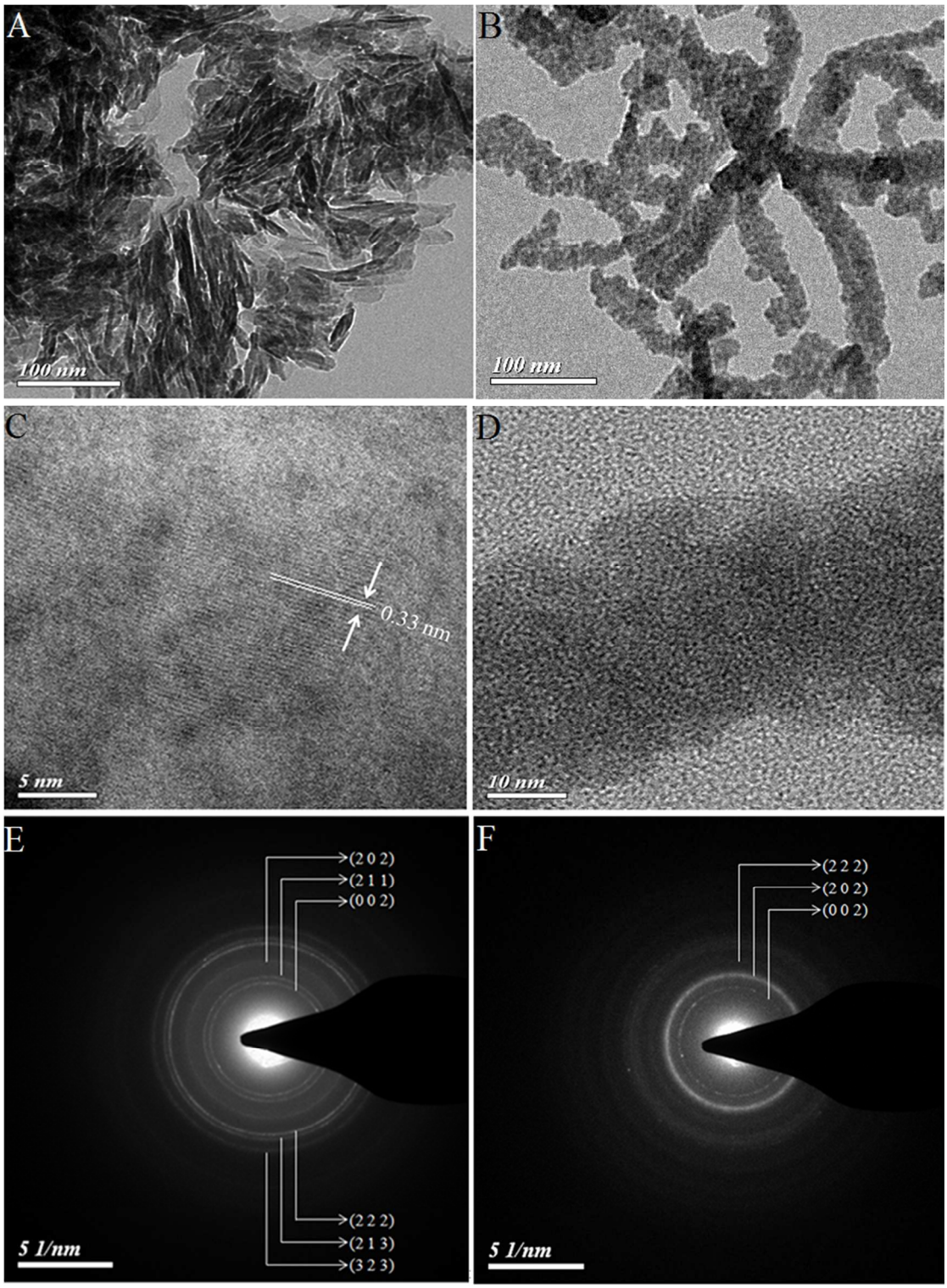

Figure 3. Figure caption. TEM images of (A) pure HAP and (B) insHAP. The grains of pure HAP and insHAP were all needle-like in shape. The grains of synthesized insHAP appeared to have a longer c-axis, like an extension. Lattice image of (C) pure HAP with a (002) d-spacing of 0.33 nm, and (D) insHAP that showed the absence of a clear lattice on the TEM due to lower crystallinity. Electronic diffraction pattern of (E) pure HAP and (F) insHAP, in which the ring pattern from the polycrystalline of pure HAP was easily identifiable, but the ring pattern from insHAP was broadened and blurry due to lower crystallinity.

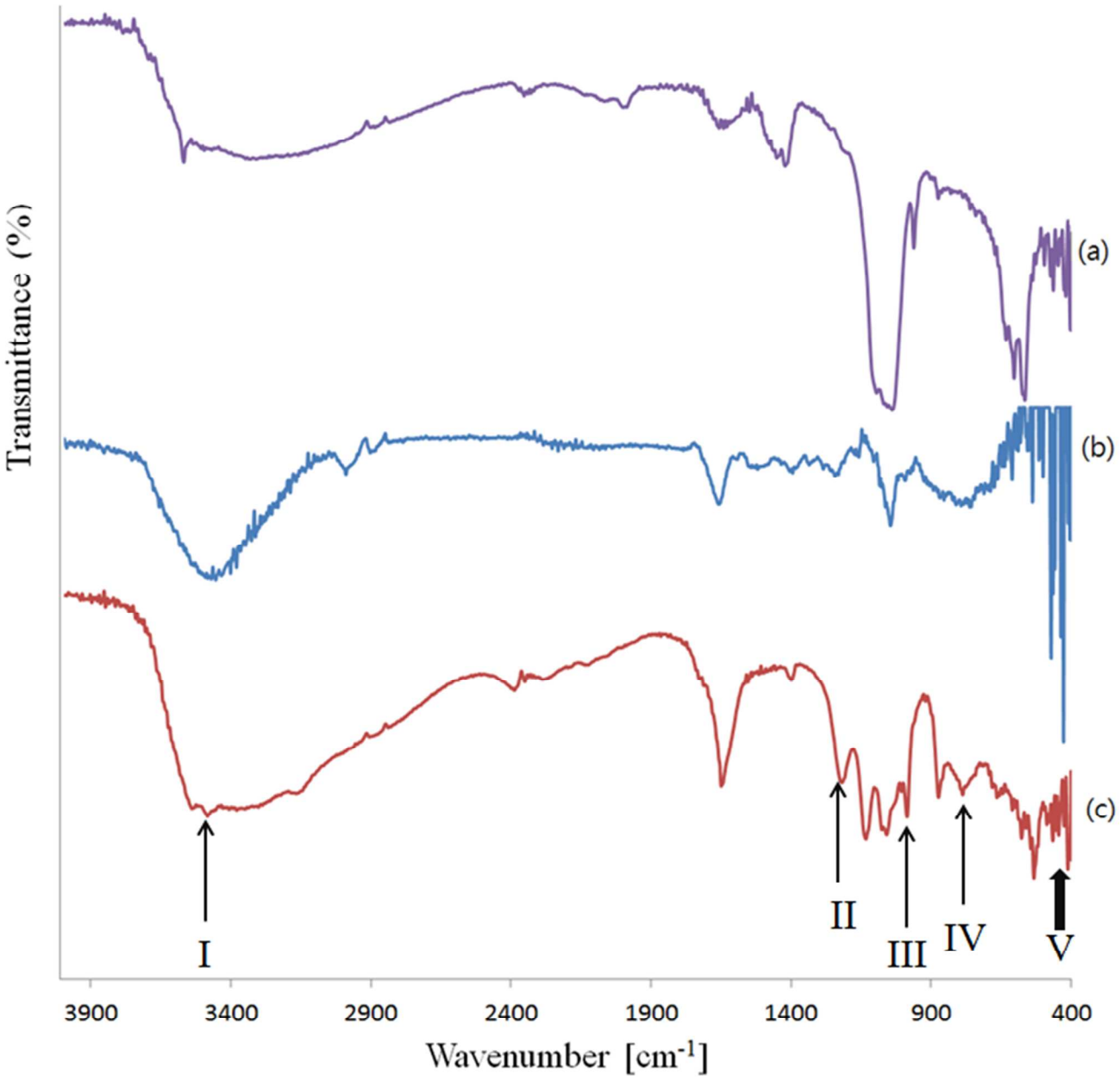

Figure 4. Figure caption. FTIR spectrophotography of (a) HAP, (b) pure insulin and (c) insHAP; where the major absorption bands were identified as I, –NH; II, –C–OH; III, C–N; IV, Aryl–NH_2; V, –S–S.

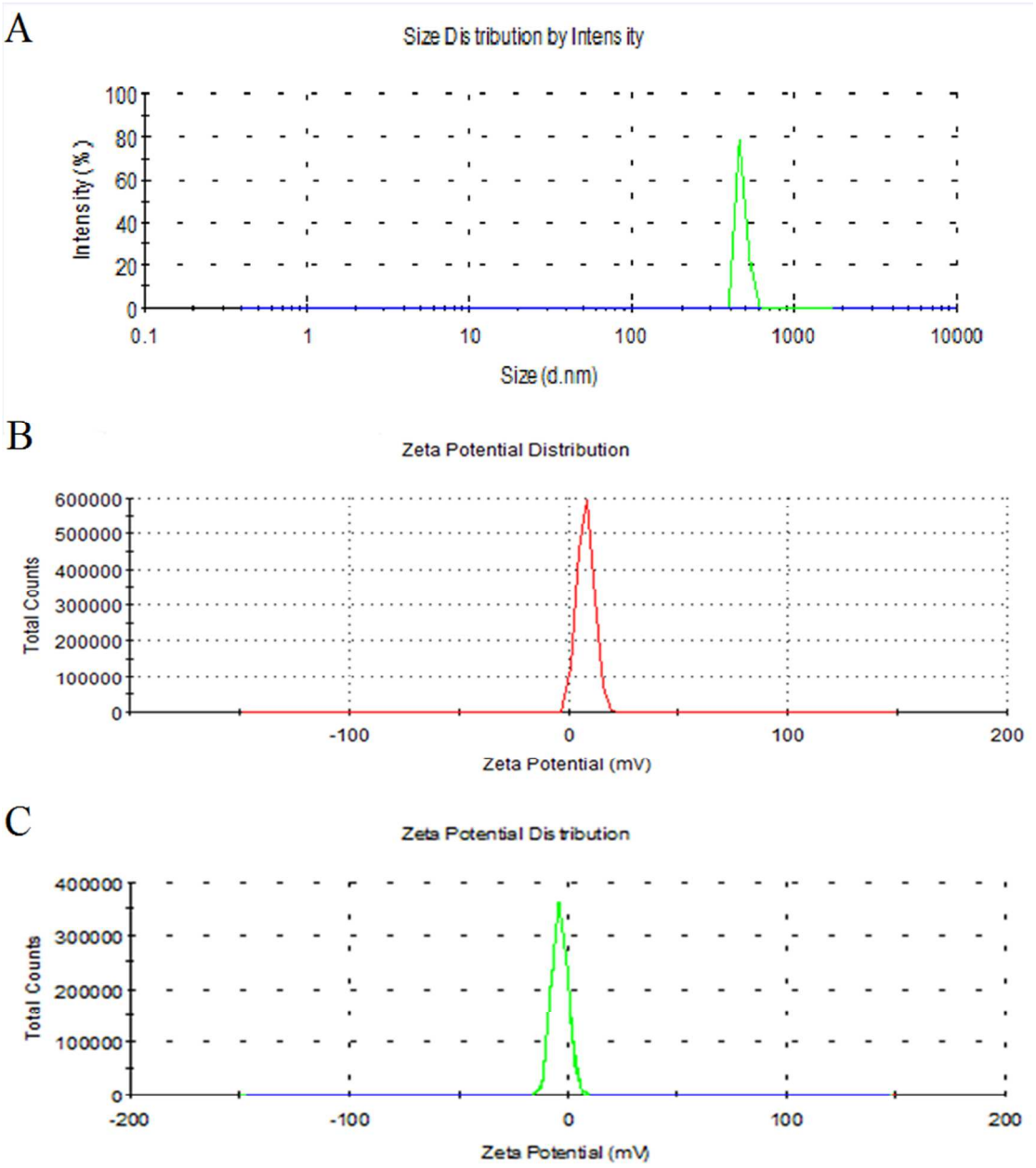

Figure 5. Figure caption. (A) Size distribution of insHAP analyzed using the zeta-sizer; the particle size was in the range of 550–865 nm. The zeta potentials of (B) pure HAP and (C) insHAP were 7.68 mV and -3.32 mV, respectively.

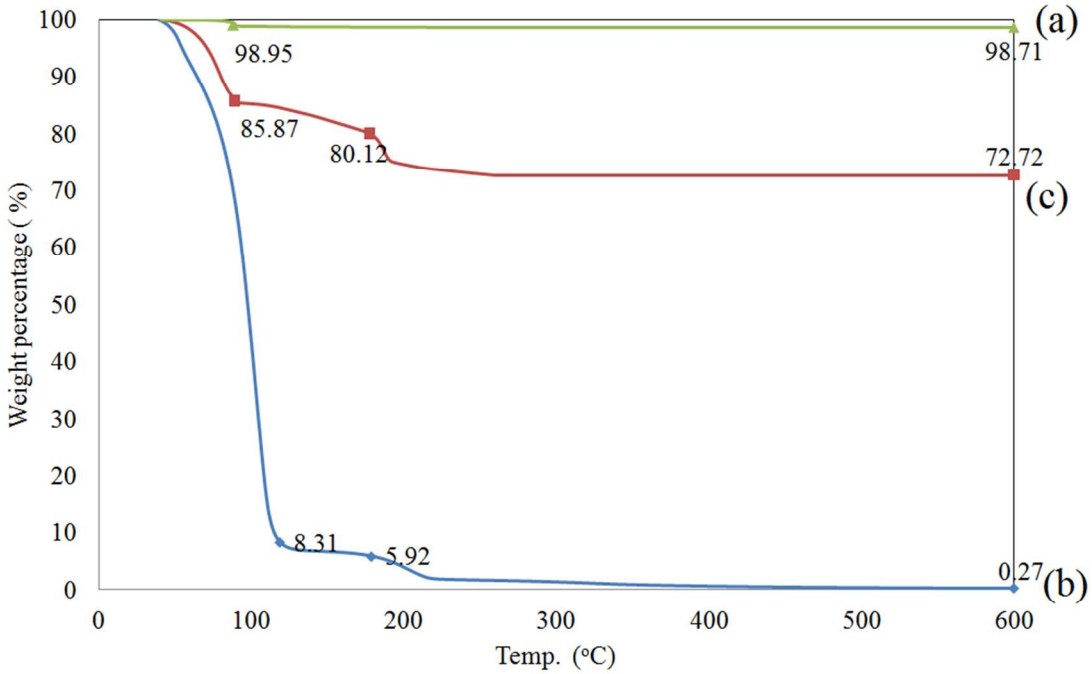

Figure 6. Figure caption. (a) Thermal analysis of pure HAP analyzed by TGA. Only minor weight loss was observed at 100°C and was due to water evaporation. (b) TGA curve of pure insulin with an initial weight loss at 100°C due to water evaporation. The second loss occurred at 225°C, which is the decomposition temperature of insulin. (c) TGA curve of insHAP shows that a 7.4% weight loss occurred at 225°C; that was related to the percentage of insulin loaded in HAP.

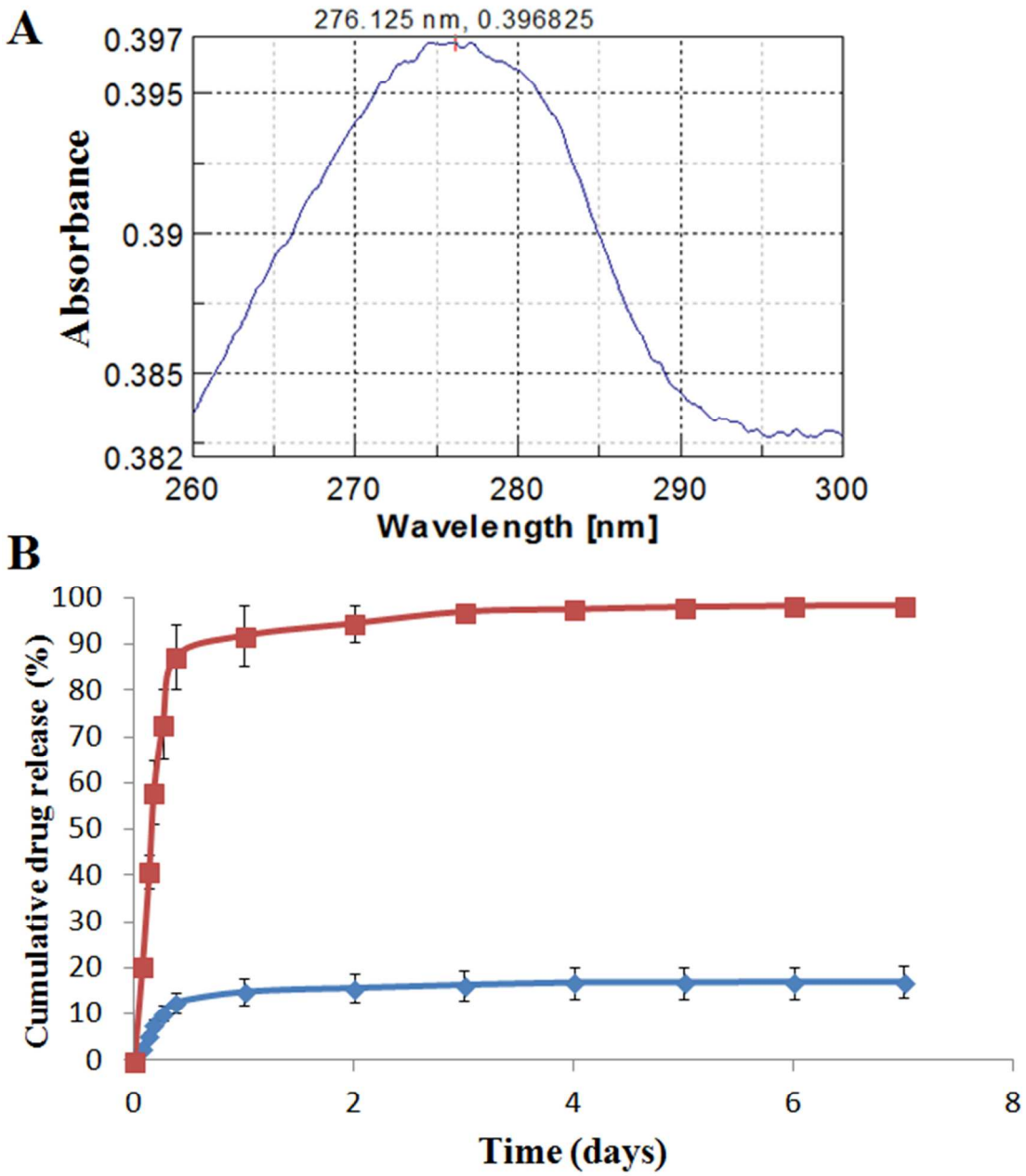

Figure 7. Figure caption. (A) UV-vis absorption curve of Humulin® R in the range of 260–300 nm. (B) Insulin release profile of insHAP. At pH 7.4, 12% of insulin was released from insHAP within the first few hours; no insulin was released from insHAP thereafter. At pH 4.0, insHAP would be dissolved, releasing 92% insulin within 2 hours and 100% by day 3.

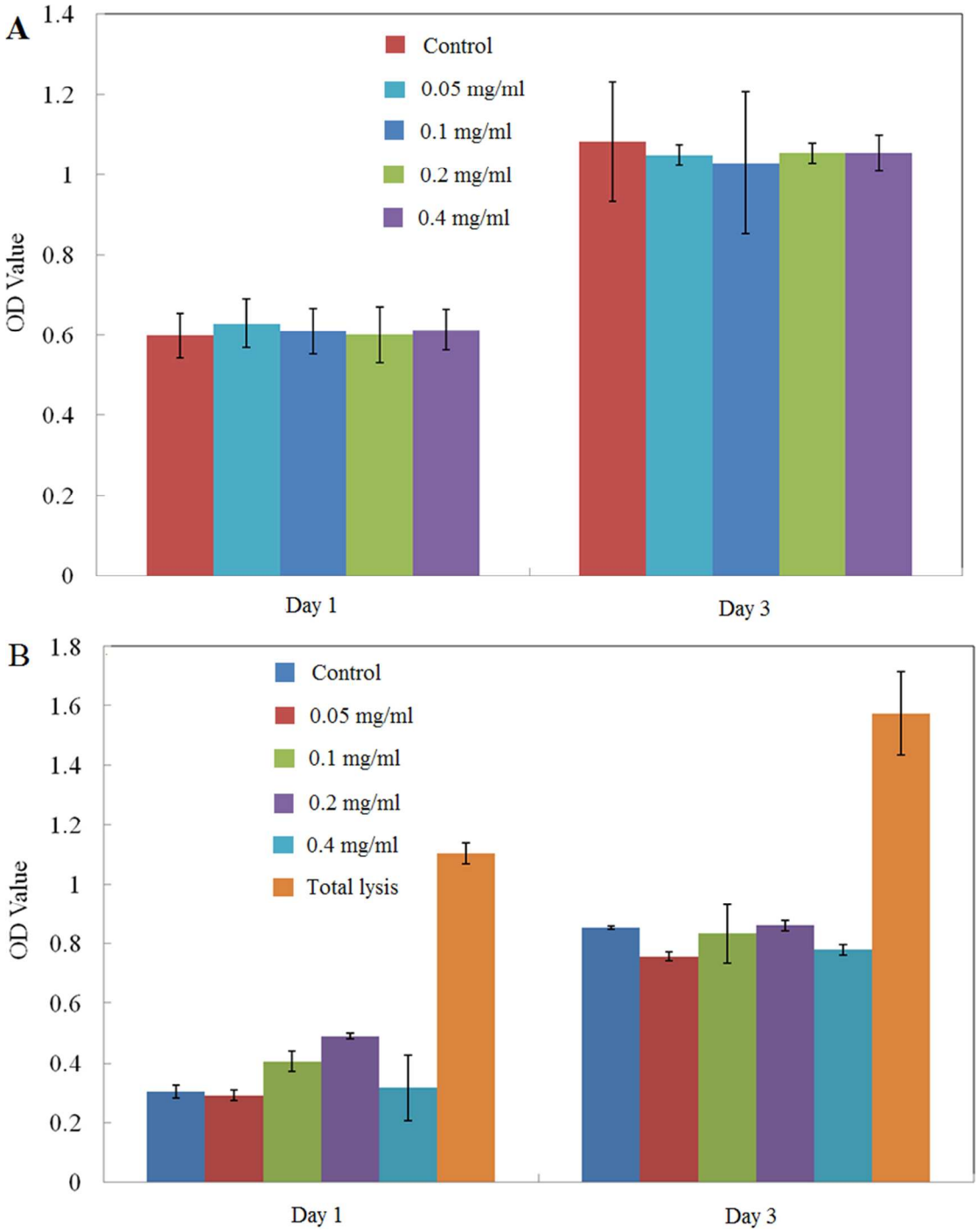

Figure 8. Figure caption. (A) WST-1 assay and (B) LDH assay in 3T3 cells treated with different concentrations of insHAP on day 1 and day 3 (n = 3)

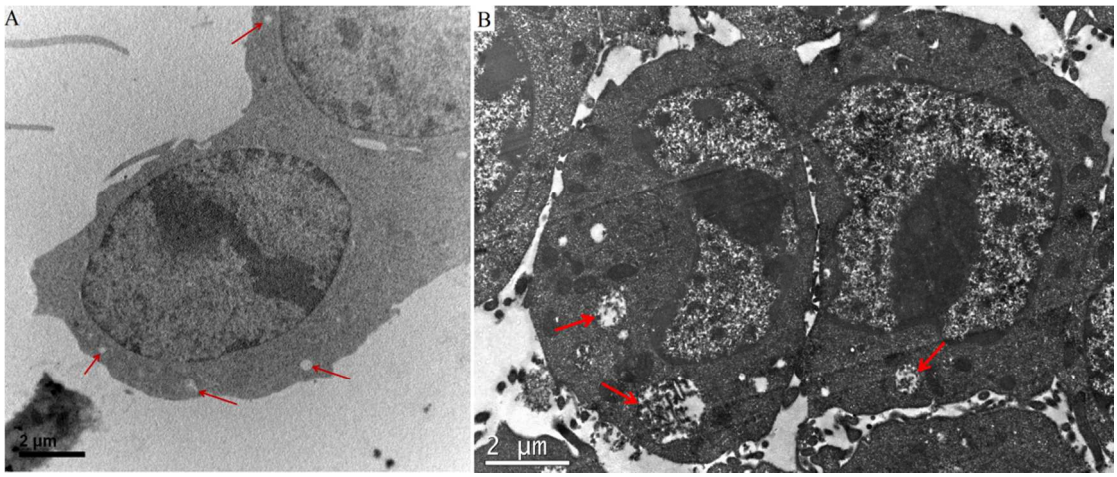

Figure 9. Figure caption. (A) RAW-264.7 cell (control) TEM samples were stained with uranyl acetate (UA) and lead citrate (LC) shown at the magnification of 12K. The lysosome/endosome hybrids (indicate by red arrows) were clean and much smaller before the uptake of insHAP particles. (B) After culturing with insHAP for 24 h, evidence of insHAP particles uptake by RAW-264.7 cells. Particles enclosed in the lysosome/endosome hybrid are shown at the magnification of 12K; red arrows indicate lysosome/endosome hybrids and black colored needle-like particles are insHAP.

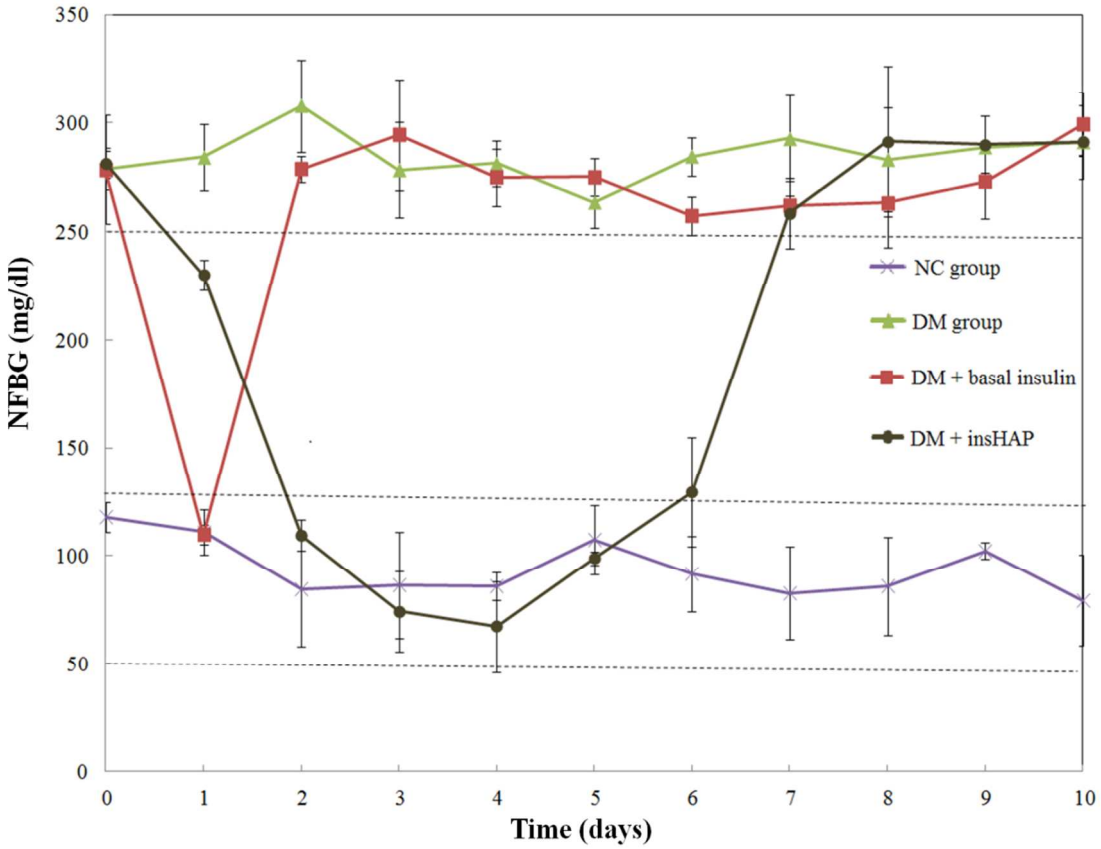

Figure 10. Figure caption. *In vivo* blood glucose measurement in various treatment groups. Blood glucose levels of DM rats treated with insHAP decreased to within the normal range by day 2 and this was maintained until day 6.

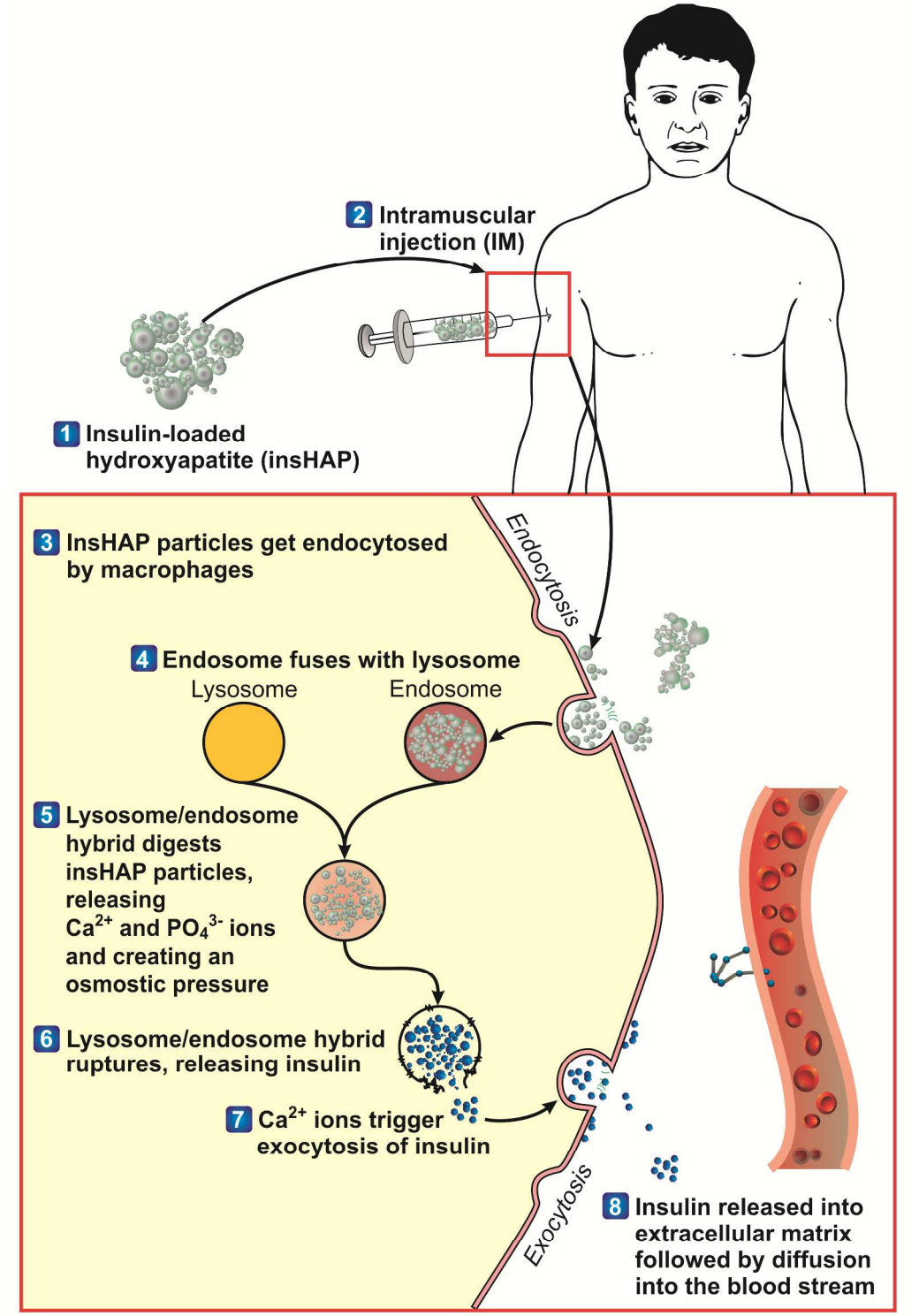

Scheme 1. Scheme Title. Schematic illustration of insulin release from insHAP, escape from lysosome/endosome hybrid, exocytosis into the extracellular matrix, and delivery to the blood circulation system.

Table 1. The summary of the 2θ shift of characteristic peaks; and the length of a-axis and c-axis of insHAP based on the XRD pattern.

Sample	**2Θ at (002)**	**shift**	**d-spacing**	**2Θ at (211)**	**shift**	**d-spacing**
HAP	25.93°	-	3.44	31.82°	-	2.82
insHAP	25.67°	-0.26°	3.47	31.61°	-0.21°	2.83
Sample	**2Θ at (300)**	**shift**	**d-spacing**	**a**	**c**	**Crystallinity**
HAP	32.90°	-	2.72	9.42	6.88	36.2%
insHAP	32.58°	-0.32°	2.74	9.46	6.94	23.7%

Table 2. Table Title. The chemical composition of insHAP from EDS analysis by weight ratio and atomic ratio.

insHAP		
Element	Weight%	Atomic%
C	6.60	10.72
N	4.27	5.95
O	50.87	62.00
P	19.05	11.99
S	0.00	0.00
Ca	19.20	9.34
Totals	100.00	100.00

Table of Contents:

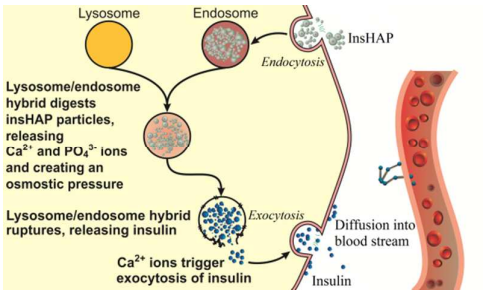

InsHAP would be engulfed by macrophage and broken down lysosome/endosome hybrid by osmosis; with which delivered insulin into blood circulation.